RSC Advances

PAPER

View Article Online
View Journal | View Issue

Cite this: *RSC Adv.*, 2015, **5**, 78738

Response of zeta potential to different types of local membrane fouling in dead-end membrane filtration with yeast suspension

Hui Jia,*[ab] Hongmei Zhang,[b] Jie Wang,[ab] Hongwei Zhang[a] and Xinbo Zhang[c]

Received 30th June 2015
Accepted 18th August 2015

DOI: 10.1039/c5ra12668a

www.rsc.org/advances

The zeta potentials that responded to different types of local membrane fouling with yeast suspension were investigated by monitoring both local flux and local zeta potential. Experiments adopting segmentation and *in situ* monitoring methods during the dead-end hollow membrane filtration process were conducted. Comparing the model with experimental data, it was found that the zeta potential reflected the type of local membrane fouling. The variations in zeta potential during membrane filtration led to different performances in pore blocking, cake formation and cake compression processes. When the zeta potential decreased rapidly, pore blocking occurred. As the zeta potential dropped gradually and linearly, it led to cake filtration. Subsequently, when zeta potential stabilized cake compression occurred. Furthermore, the effect of fiber length on local fouling behavior was also studied. With an increase in fiber length, the time taken by the three segments to enter the cake layer compression stage was extended, and the difference between the zeta potential values in the three segments tended to increase.

1. Introduction

Membrane application in water treatment provides many advantages over conventional treatment processes. However, membrane fouling is an inevitable problem impairing all membrane processes, as it leads to reduced permeate flux, increased energy demand, higher maintenance costs, and decreased membrane lifetime, which restricts the widespread applications of membranes.[1,2]

Membrane fouling is generally observed as a flux decline during membrane filtration. Fouling phenomena can be evaluated by analyzing experimental flux decline data and filtration models.[3,4] The flux decline in dead-end filtration can be explained by classical fouling models including pore constriction (standard blocking),[5] complete pore blockage, intermediate pore blockage,[6] cake formation[7] and some combined models that integrate two or more of the above.[8,9] It is very simple to understand membrane fouling mechanisms using the above models to analyze flux data, but the actual membrane fouling process is more complicated than that defined according to the hypotheses of these models. In order to understand membrane fouling in depth, some online monitoring methods with flux decline measurements have been proposed, such as optical imaging,[10] ultrasonic time domain reflectometry,[11,12] cake layer thickness measurements,[13] and surface charge character measurements.[14,15] Particle deposition can be clearly observed by optical imaging techniques, but the observation has its limitations, that is, the image is only focused on the membrane surface (flat-sheet membranes) or on the side view of the hollow fiber cross-section (hollow fiber membranes). In addition, it has a high testing cost. Li *et al.*[11,12] used a single hollow fiber membrane inserted into two thin polyurethane (PU) hosepipes, in which the interspaces between the fiber and hosepipe were blocked off with epoxy resin, to study local fouling distribution along the fiber. However, there was still a deviation between the measurement results and real operational data acquired in the membrane filtration process. It is necessary to point out that ionic deposition and electrokinetic phenomena are not just problems for single membrane fibers.

The surface charge conditions of membranes, which provide useful information about the electrostatic interactions between membrane and foulants, are an important parameter in fouling studies. In recent years, several researchers have employed the membrane zeta potential as a key parameter to study the fouling characteristics of different types of membrane. The changes in zeta potential between fouled membranes and clean membranes can be used to monitor membrane fouling.[16] Y. Soffer *et al.*[17] applied a method to study the fouling of polysulfone ultrafiltration membranes with different molecular weight cut offs, employing coupling flux with the streaming potential method. This demonstrated that two fouling layers formed on original and fouled membranes had different

[a]*State Key Laboratory of Separation Membranes and Membrane Processes, Tianjin Polytechnic University, Tianjin 300387, China. E-mail: ajiahui@163.com; Fax: +86 022 8395 5668; Tel: +86 022 8395 5668*

[b]*School of Environmental and Chemical Engineering, Tianjin Polytechnic University, Tianjin 300387, China*

[c]*School of Environmental and Municipal Engineering, Tianjin Chengjian University, Tianjin 300384, China*

features. It also showed a linear relationship between the change in zeta potential from the clean to the fouled membrane and the degree of fouling. Furthermore, M. S. Chun *et al.*[18] researched the evolution of streaming potential coefficient during BSA suspension filtration. They detected a decrease in the streaming potential coefficient from a positive value to a negative one as time went on, which meant that the electrostatic repulsion made the BSA particles collect mainly in the concentration polarization layer instead of being deposited onto the outer surface of the hollow fiber. Furthermore, they found that the time evolution of the streaming potential was closely related to the filtrate flux decline. The same phenomenon was also found by B. Teychene *et al.*[16] Z. P. Zhao *et al.*[15] showed that the flux and streaming potential methods were complementary in examining the mechanism of charged membrane fouling, and could provide more microscopic information, which helped them to understand the fouling mechanism between material and membrane. Nevertheless, these reports scarcely studied the zeta potential changes in different segmented membrane fibers to further understand the membrane filtration process.

This study employed local zeta potential with local flux to *in situ* monitor types of local fouling in horizontal dead-end hollow fiber membrane modules divided into three sections (namely upstream, middle, and downstream) under constant pressure operation. The combined model was adopted to analyze the flux data. The effect of fiber length on types of local fouling was also investigated. It was expected that the formation process of local membrane fouling could be described by the response of the zeta potential.

2. Experimental

2.1. Membrane and feed suspension characteristics

Polyvinylidene fluoride (PVDF) hollow fiber membranes (Tianjin Motimo Membrane Technology Co. Ltd., China) with a nominal pore size of 0.22 μm, and inside and outside diameters of 0.6 mm and 1.1 mm respectively, were used in this study. Each membrane module was soaked with deionized water for at least 24 h to remove the wetting agent prior to use. The experiments adopted the external pressure membrane filtration process.

The fouling experiments were carried out with 0.5 g L^{-1} yeast suspension in order to generate an appropriate rate of membrane fouling during ultrafiltration experiments. All runs were carried out at room temperature (20 ± 2 °C). Before utilization, active dry yeast (AngelYeast Co. Ltd., China) cells were washed three times with deionized water, centrifuged and dried at 80 °C for 24 h in a hot air oven to deactivate the cells,[19] then suspended in distilled water. After processing, their mean diameter was 5.4 μm. The particle size was tested with a laser scattering particle size distribution instrument (Mastersizer 2000, Malvern, UK). The solution was appropriate for the performance analysis of the membrane filtration.

In order to carry out surface charge characterization of the yeast solution and clean membrane, the zeta potentials of the yeast solution and clean membrane under different pH conditions were measured using Zeta-Plus (Zetasizer nano ZS90, Malvern Instruments, UK and PALS, Brookhaven Instruments Corp., USA).

As shown in Fig. 1, the zeta potentials of the yeast solution and the clean membrane change from positive to negative with the increase of pH. The isoelectric points of the yeast solution and clean membrane are around pH 3.8 and 4.2, respectively. The pH of the yeast solution used in this study was 6.1 (yeast solution is prepared directly, without acid or alkali). From Fig. 1, the zeta potential of the yeast solution was −18.5 mV, while the clean membrane was −6.1 mV at this pH. The data show that the yeast solution and the surface of the membrane pore wall are both negatively charged at a pH of 6.1.

2.2. Simultaneously monitoring local flux and zeta potential systems

A schematic diagram of the system for simultaneous monitoring of local flux and zeta potential is shown in Fig. 2. Three feed sinks were connected in series with the membrane module inserted by a quick pipe connector. A constant pressure pump (TP 10–20, Motimo, China) was used to drive the constant overall pressure. Three pairs of commercial Ag/AgCl electrodes (218 reference electrode, Shanghai Leici, China) were placed on the permeate and retentate sides, which were close to the membrane module.[20] The electrodes were connected to a data acquisition system (USB-FS1208, Measurement ComputingTM, Hungary) that recorded experimental data once every 4 min automatically. The changes in transmembrane pressure (TMP) of the three membrane sections were monitored using pressure sensors (Danfoss, MBS 3000, Denmark) that recorded once automatically every 4 min with a paperless recorder (MIK210B, MEACON, China). Integrated data processing software recorded the variation in electronic balance (CN-AS, Taiwan Yinghua, China), which measured the effluent weight once every 4 min and transformed it into membrane flux. It was noteworthy that the liquid levels of three tanks were kept relatively constant

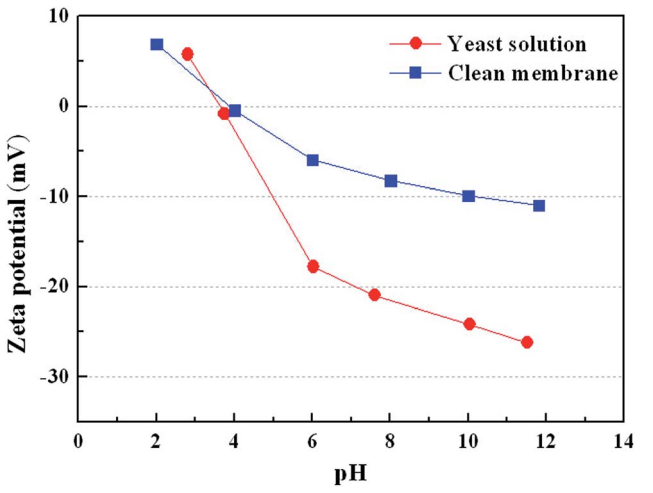

Fig. 1 Zeta potential characterizations of yeast solution and clean membrane in 1.0 mM KCl solution.

manually. An air pump (ACO-818, Sensen Industry Co. Ltd., Zhoushan, China) worked at a certain rate of aeration to prevent the sedimentation of the feed suspension. All the experiments were repeated at least five times.

2.3. The calculation of the zeta potential

Electrokinetic techniques such as streaming potential measurements have been applied in the characterisation of the surface charge condition of membranes, and the streaming potential can be monitored during filtration. The fundamental relationship between the measured streaming potential and the membrane zeta potential is given by the well-known Helmholtz–Smoluchowski (H–S) equation ((1)):[20,21]

$$\frac{\Delta P}{\Delta E} = \frac{\varepsilon \varepsilon_0 \xi}{\mu \lambda}, \quad (1)$$

where ΔE is the streaming potential difference, mV; ΔP is the transmembrane pressure drop, Pa; ε is the relative dielectric constant of the electrolyte solution; ε_0 is the vacuum dielectric constant, s m^{-1} Ω^{-1}; ξ is the zeta potential, mV; μ is the solution viscosity, Pa s; λ is the solution conductivity, 1/m Ω. The electrolyte solution was 1.0 mM KCl. Moreover, eqn (1) is restricted to the limit of $r_P/\kappa^{-1} > 10$ (r_p is pore radius, m; κ^{-1} is Debye length, m). In this study, $r_P/\kappa^{-1} = 22.85 > 10$, eqn (1) is applicable to calculate the zeta potential.

It should be pointed out that the membrane zeta potential determined from eqn (1) is an apparent value. This paper puts emphasis on the change in zeta potential over time. If a more rigorous zeta potential is needed, one could consider the corrected H–S equation.[17]

2.4. Fouling model

Plenty of studies have established mathematical models to investigate the forms of membrane fouling,[3–5,22,23] among them a widely used and simple combined fouling model to analyze flux decline data is a t/V *vs.* V plot, shown in Fig. 3, where t is filtration time and V is the permeate volume.

The t/V *vs.* V plot typically shows three regions in membrane filtration that correspond to (i) blocking filtration, (ii) cake filtration, and (iii) cake clogging and/or cake compression. The initial curve depicting a gradual reduction in the slope with increasing V results from a pore blocking mechanism. The linear part characterizes well the filtration mechanism of cake filtration. The final part of the curve, which indicates a considerable increase in flow resistance, may arise from the

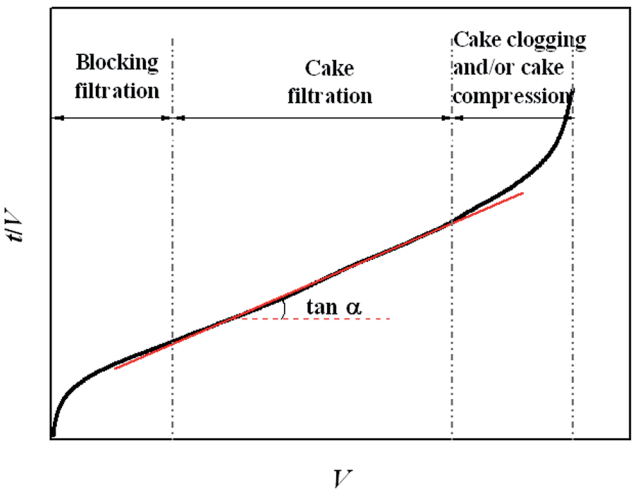

Fig. 3 Ratio of filtration time and volume (t/V) *vs.* filtrate volume (V).[22]

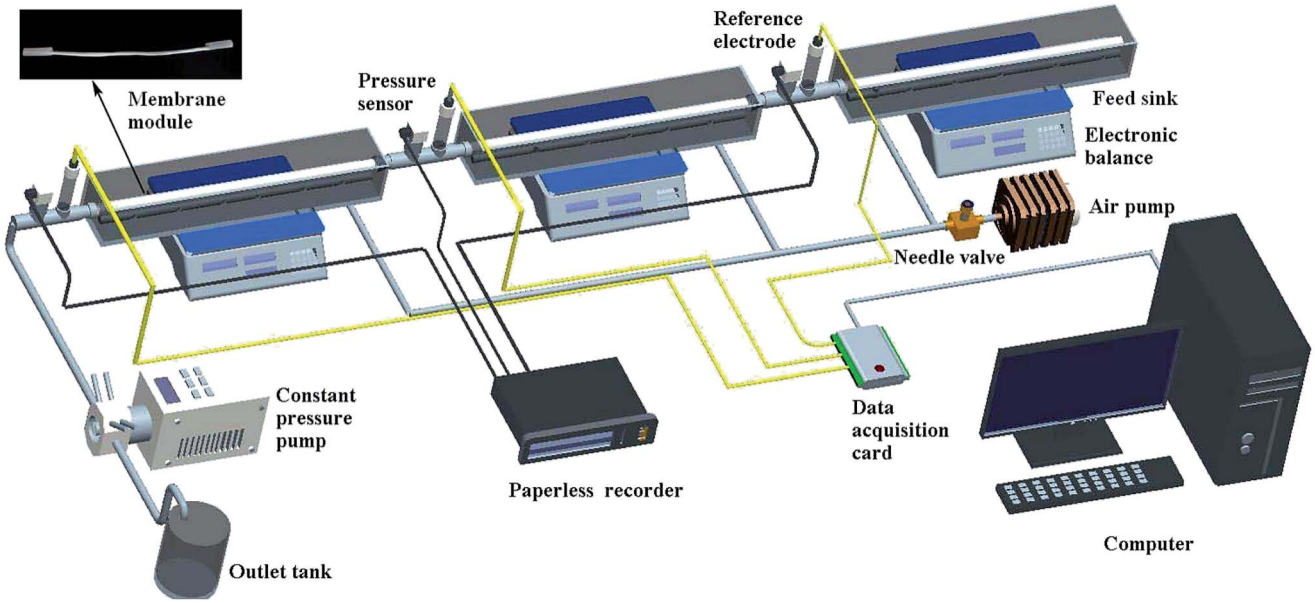

Fig. 2 Experimental apparatus for simultaneously monitoring local flux and zeta potential.

formation of a compressible cake or from subsequent clogging of cake flow passages.[22]

3. Results and discussion

3.1. Section characterization of different types of local fouling by zeta potential and local flux

From the overall point of view, it can be seen in Fig. 4 that both the local flux and zeta potential decrease along the membrane filtration process due to the fact that the fouling resistance increases. No matter which parts of the membrane (upstream, middle, or downstream), the time evolution of the zeta potential was closely related to the filtrate flux decline. The same phenomena were also found by Y. Soffer *et al.*[17] and J. H. Sung *et al.*[14] Additionally, it can be observed that the zeta potential values vary between clean membrane and yeast solution.

The absolute values of zeta potential were larger in the upstream. This might be due to the fact that the negatively charged yeast particles were hardly deposited onto the outer surface of the negatively charged hollow fiber membrane, and were in fact deposited on the concentration polarization layer that was suspended on the membrane surface. Moreover, uneven driving force and shear force would lead to greater concentration polarization in the upstream than the middle.[20] The feed permeate rate increases as it goes upstream due to radial permeation, and thus the pressure drop changes.[24]

As shown in Fig. 4, the zeta potentials of the three sections dropped quickly in the initial few minutes, then gently declined until the end. The rapid drop in the zeta potentials in the initial few minutes might be due to pore blocking. It could also be attributed to the electrostatic repulsion between charged membrane surface and yeast suspension, the formation of a double electrode layer, as well as concentration polarization. Then followed the cake filtration process.[25] The formation of a cake layer prevented the further blocking of the membrane pores, so the zeta potential values of the three sections tended to decrease more gently, which was attributed to the weakened electrokinetic flow resulting from the narrowed membrane pores, due to the continued deposition of yeast particles. As membrane filtration continued, the zeta potential values of the three sections appeared to stabilize, which might indicate the beginning of the cake layer compression stage.

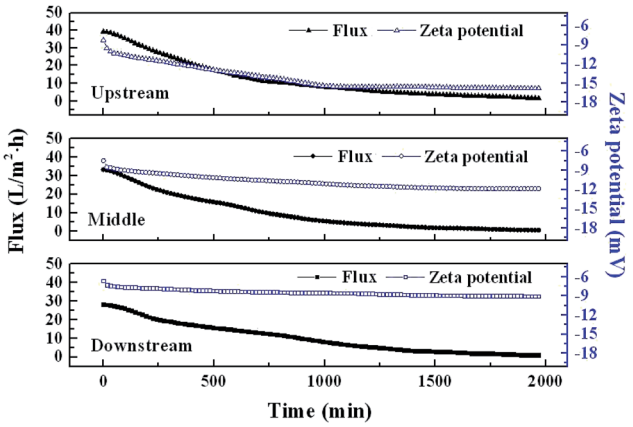

Fig. 4 Flux and zeta potential variations of the three parts of the membrane module against filtration time at a fiber length of 1.2 m and a TMP of about 0.50 bar.

Combining the flux data of the three segments, and referring to the model established in Fig. 3 while contrasting Fig. 3 and 5(a), it can be concluded that pore blocking occurred in a short period at the beginning of the filtration, followed by cake formation and then cake compression. Coupled with the zeta potential data in Fig. 5(b), it can be seen that the zeta potential rapidly decreased in the early stages of the filtration and then dropped gradually and linearly until being almost stable at the end of membrane filtration, which meant that membrane filtration experienced pore blocking, cake filtration and cake compression. The conclusions regarding pore blocking and cake filtration were consistent with the research of K. Nakamura *et al.*[25] Nevertheless, they assumed the zeta potential jumped from that of a clean membrane to a certain value between this and the cake layer's zeta potential as filtration started, and became nearly stable in the pore blocking filtration, followed by the cake filtration. What is more, the existence of cake layer compression has not been taken into account yet.

In the filtering process, the upstream section entered the cake formation and cake compression stages first. The periods of time before entering the cake formation stage for the upstream, middle and downstream sections were $t_{U1} = 20$ min, $t_{M1} = 22$ min, $t_{D1} = 24$ min, respectively, and those for the cake compression stage were $t_{U2} = 1032$ min, $t_{M2} = 1112$ min, $t_{D2} = 1240$ min, respectively, when fitting the data of the cake formation stage to the obtained linear equations ($R_U^2 = 0.9249$, $R_M^2 = 0.9125$, $R_D^2 = 0.8857$). This indicated that cake formation and cake compression in the middle section occurred as early as in the downstream section, because the internal pressure in the fiber lumen dropped from the upstream to the downstream section during the dead-end hollow fiber membrane filtration process.

3.2. Effect of fiber length on the different types of local fouling

In the case of a constant TMP of 0.35 bar, the local zeta potential variations in different fiber lengths (0.6, 1.2, 1.8 m) were investigated to study the effect of fiber length on the different types of local fouling.

As shown in Fig. 6(a) and (c), the upstream section first entered the cake layer formation stage, because the suction pressure was largest near the pump in the conditions of dead-end filtration. However, when the fiber length was increased to 1.8 m, as shown in Fig. 6(e), the downstream section entered the cake layer formation stage first, because the fiber length was so long that the local flux in the downstream section decreased very slowly and almost underwent no change at first, and the ratio of t/V *vs.* V increased sharply. With increasing fiber length, the periods of time before entering the cake compression stage at the upstream, middle and downstream sections were $t_{U2\text{-}0.6} = 1128$ min, $t_{M2\text{-}0.6} = 1208$ min, $t_{D2\text{-}0.6} = 1256$ min, $t_{U2\text{-}1.2} = 1208$ min, $t_{M2\text{-}1.2} = 1304$ min, $t_{D2\text{-}1.2} = 1400$ min, $t_{U2\text{-}1.8} = 1320$ min,

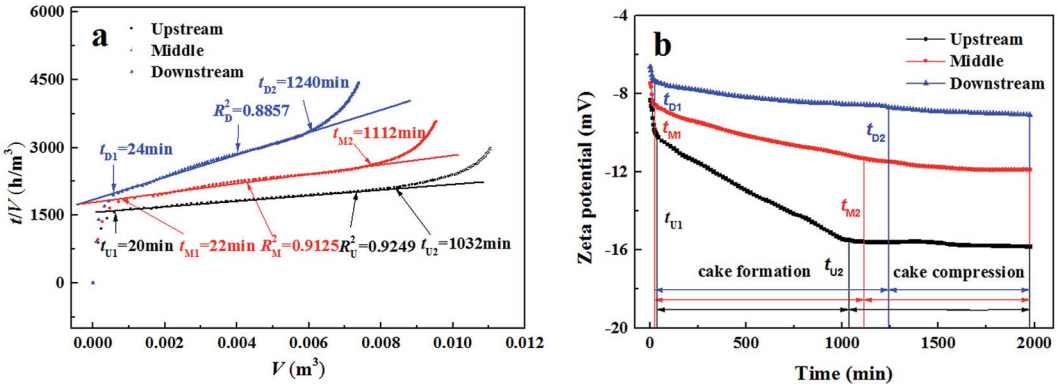

Fig. 5 Ratio of *t*/*V* *vs.* *V* (a) and zeta potential against filtrate time (b) for the upstream, middle and downstream sections at 1.2 m fiber length and a TMP of about 0.50 bar.

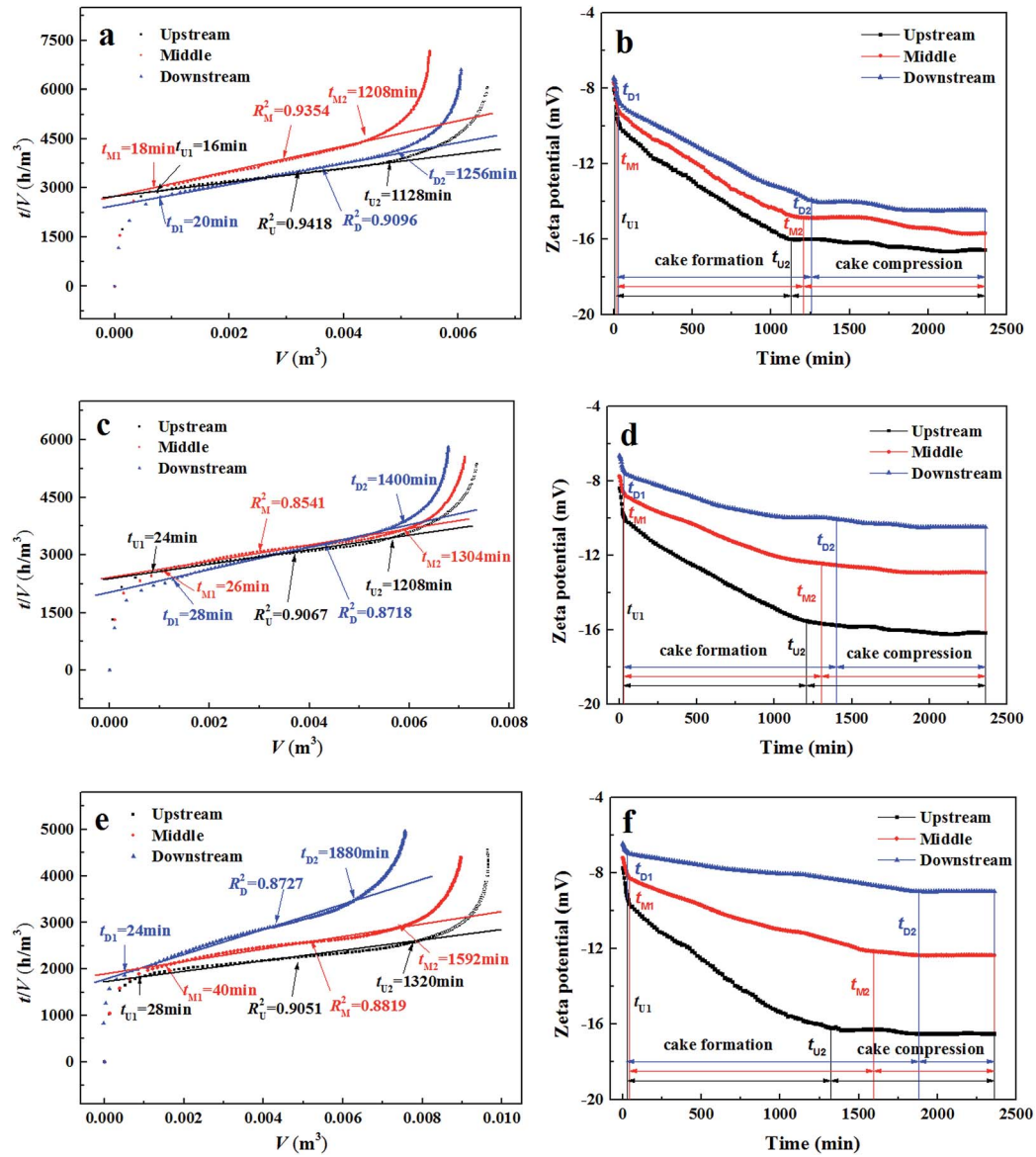

Fig. 6 Ratio of *t*/*V* *vs.* *V* (a, c and e) and zeta potential against filtrate time (b, d and f) in the upstream, middle, and downstream sections with different fiber lengths (0.6 m, 1.2 m, 1.8 m) at about 0.35 bar.

$t_{M2\text{-}1.8}$ = 1592 min, $t_{D2\text{-}1.8}$ = 1880 min, respectively. The time period before entering the cake compression stage was extended obviously as fiber length increased. However, no matter how long the fiber length was, the upstream section always entered the cake compression stage first. This was because the internal pressure in the fiber lumen dropped from the upstream to the downstream section during the dead-end hollow fiber membrane filtration process, which led to uneven fouling distribution and the possibility of a fouling redistribution phenomenon occurring.

Compared with the zeta potential data in Fig. 6(b), (d) and (f), it also could be seen that the zeta potential values varied between clean membrane and yeast solution. Furthermore, with the increase in fiber length the zeta potential difference values of the three segments tended to increase. The main reason for this was the uneven hydrodynamic distribution along the fiber, including TMP and local flux, leading to an uneven distribution of concentration polarization and membrane fouling. According to the uneven fouling theory of hollow fiber membranes,[26] fouling resistance increases gradually throughout membrane filtration, which results in the uneven distribution of local flux. The longer the membrane fiber is, the greater the unevenness of the local flux. Therefore, the zeta potential difference values of the three segments tended to increase. The growth of the cake layer had indeed slowed with the increase of fiber length, and the weakened electrokinetic flow owing to a lower permeate flux led to a decrease of the membrane zeta potential.

In summary, the zeta potential values did reflect the different types of local membrane fouling. When the zeta potential rapidly decreased, pore blocking occurred. In the cake filtration stage, the zeta potential declined gradually and linearly, while the zeta potential was almost stable when cake compression occurred.

4. Conclusions

The responses of zeta potential to local membrane fouling behavior were studied by monitoring both local flux and local zeta potential during dead-end membrane filtration. The zeta potential changes during membrane filtration were quite different for the pore blocking, cake formation and cake compression processes. The zeta potential was rapidly decreased during the pore blocking process, but in the cake formation process the zeta potential declined gradually and linearly, while the zeta potential was almost stable during the process of cake compression.

During the process of dead-end membrane filtration, the zeta potential values ranged between clean membrane and filtration solution. In addition, fiber length had a significant impact on local zeta potential distribution and the different types of local membrane fouling. With the increase in fiber length, the time taken for the three segments to enter the cake compression stage was extended and the zeta potential difference values of the three segments tended to increase. This study provides new insights in membrane fouling measurement, which could be advantageous for the understanding of the characteristics of the membrane fouling process.

Acknowledgements

This study was financially supported by the National Natural Science Foundation of China (No. 51378349), the China Postdoctoral Science Foundation (2013M541184), and the Program for Changjiang Scholars and the Innovative Research Team at the University of Ministry of Education of China (Grant No. IRT13084).

References

1 K. J. Martin, D. Bolster, N. Derlon, E. Morgenroth and R. Nerenberg, *J. Membr. Sci.*, 2014, **471**, 130–137.
2 K. J. Howe and M. M. Clark, *Environ. Sci. Technol.*, 2002, **36**, 3571–3576.
3 L. F. Song, *J. Membr. Sci.*, 1998, **139**, 183–200.
4 T. Mohammadi, M. Kazemimoghadam and M. Saadabadi, *Desalination*, 2003, **157**, 369–375.
5 G. Bolton, D. LaCasse and R. Kuriyel, *J. Membr. Sci.*, 2006, **277**, 75–84.
6 M. C. V. Vela, S. A. Blanco, J. L. García and E. B. Rodríguez, *Sep. Purif. Technol.*, 2008, **62**, 489–498.
7 J. Shin, K. Kim, J. Kim and S. Lee, *Desalination*, 2013, **309**, 213–221.
8 C. C. Ho and A. L. Zydney, *J. Colloid Interface Sci.*, 2000, **232**, 389.
9 G. Bolton, D. LaCasse and R. Kuriyel, *J. Membr. Sci.*, 2006, **277**, 75.
10 C. Dreszer, A. D. Wexler, S. Drusová, T. Overdijk, A. Zwijnenburg, H.-C. Flemming, J. C. Kruithof and J. S. Vrouwenvelder, *Water Res.*, 2014, **67**, 243–254.
11 X. H. Li, J. X. Li, J. Wang, H. Wang, B. Q. He, H. W. Zhang, W. S. Guo and H. H. Ngo, *J. Membr. Sci.*, 2014, **453**, 18–26.
12 X. H. Li, J. X. Li, J. Wang, H. Wang, Z. Y. Cui, B. Q. He and H. W. Zhang, *J. Membr. Sci.*, 2014, **451**, 226–233.
13 J. Mendret, C. Guigui, P. Schmitz and C. Cabassud, *J. Membr. Sci.*, 2009, **333**, 20–29.
14 J. H. Sung, M. S. Chun and H. J. Choi, *J. Colloid Interface Sci.*, 2003, **264**, 195–202.
15 Z. P. Zhao, Z. Wang and S. C. Wang, *J. Chem. Eng. Data*, 2003, **54**, 417–418.
16 B. Teychene, P. Loulergue, C. Guigui and C. Cabassud, *J. Membr. Sci.*, 2011, **370**, 45–57.
17 Y. Soffer, J. Gilron and A. Adin, *Desalination*, 2002, **146**, 115–121.
18 M. S. Chun and W. C. Park, *J. Membr. Sci.*, 2004, **243**, 417–424.
19 S. Schiewer and B. Volesky, *Environ. Sci. Technol.*, 1995, **29**, 3049–3058.
20 Y. R. Qiu and J. Qi, *J. Membr. Sci.*, 2013, **425–426**, 71–76.
21 M. Nystrom, A. Pihlajamaki and N. Ehsani, *J. Membr. Sci.*, 1994, **87**, 245–256.
22 S. F. E. Boerlage, M. D. Kennedy, M. P. Aniye, E. Abogrean, Z. S. Tarawneh and J. C. Schippers, *J. Membr. Sci.*, 2003, **211**, 271–289.
23 R. van Reis and A. Zydney, *J. Membr. Sci.*, 2007, **297**, 16–50.

24 M. S. Chun, H. I. Cho and I. K. Song, *Desalination*, 2002, **148**, 363–367.
25 K. Nakamura, T. Orime and K. Matsumoto, *J. Membr. Sci.*, 2012, **401–402**, 274–281.
26 M. C. Vincent-Vela, E. Bergantiños-Rodríguez, S. Álvarez-Blanco and J. Lora-García, *Desalin. Water Treat.*, 2009, **10**, 134–138.